

# Ion-specific Interactions at Calcite-Brine Interfaces: A Nano-Scale Study of the Surface Charge Development and Preferential Binding of Polar Hydrocarbons

Mohammad Hasan Badizad<sup>1,2,†,‖</sup>, Mohammad Mehdi Koleini<sup>3,\*</sup>, H. Chris Greenwell<sup>4</sup>,

Shahab Ayatollahi<sup>3,\*\*</sup>, Mohammad Hossein Ghazanfari<sup>2</sup>, Mohsen Mohammadi<sup>1</sup>

<sup>1</sup> Department of Chemical Engineering, Isfahan University of Technology, Isfahan, Iran

<sup>2</sup> Department of Chemical and Petroleum Engineering, Sharif University of Technology, Tehran, Iran.

<sup>3</sup> Sharif Upstream Petroleum Research Institute (SUPRI), Department of Chemical and Petroleum Engineering, Sharif University of Technology, Tehran, Iran.

<sup>4</sup> Department of Earth Sciences, Durham University, Durham DH1 3LE, UK

<sup>†</sup> **Email:** [m.badizad@ce.iut.ac.ir](mailto:m.badizad@ce.iut.ac.ir), [mohammadhasan.badizad@che.sharif.edu](mailto:mohammadhasan.badizad@che.sharif.edu) & [badizad@gmail.com](mailto:badizad@gmail.com)

<sup>\*</sup> Corresponding Author; **Email:** [mmkoleini@che.sharif.edu](mailto:mmkoleini@che.sharif.edu) & [mmkoleini@gmail.com](mailto:mmkoleini@gmail.com)

<sup>\*\*</sup> Corresponding Author; **Email:** [shahab@sharif.edu](mailto:shahab@sharif.edu)

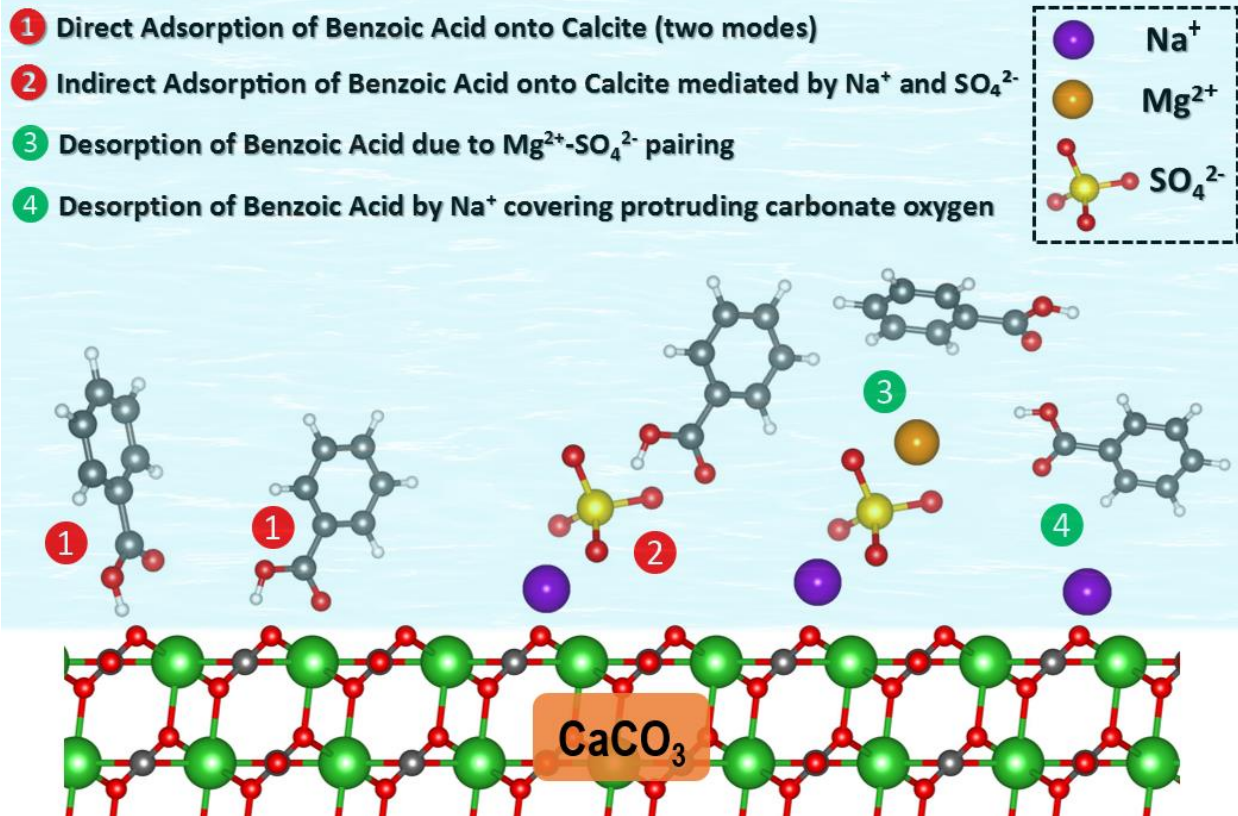
<sup>‖</sup> M.H. Badizad and M.M. Koleini contributed equally to this work.

## Abstract

This research provides an atomic-level insight into the synergic contribution of mono- and divalent ions to interfacial characteristics of calcite surface exposed to electrolyte solution containing organic compounds. The emphasis was placed on the ionic interactions responsible for charge developing mechanisms of calcite surface and also the capacity for polar hydrocarbons adsorption, represented by Benzoic acid (BA), at different brine compositions. For this purpose, Molecular dynamics (MD) simulation was employed to explore the interplay of the main constituent ions of natural brines ( $\text{Na}^+$ ,  $\text{Cl}^-$ ,  $\text{Mg}^{2+}$ , and  $\text{SO}_4^{2-}$ ) and BA at the interface of  $\text{CaCO}_3$ . It was observed that surface accumulation of  $\text{Na}^+$  cations produces a positively charged layer immediate to the basal plane of calcite, validating the typical positive surface charge of carbonates reported by laboratory experiences. Meanwhile, a negatively charged layer appears beyond the sodium layer as a result of direct and solvent-mediated pairing of anions with  $\text{Na}^+$  cations lodging on the calcite substrate. In this process, sulfate adsorption severely diminishes surface charge to even a negative value in the case of  $\text{SO}_4^{2-}$ -rich solution, providing an interpretation for the measurements reported in the literature. Our results revealed the inhibition of direct binding of BA molecules onto the calcite surface through complexation with protruding oxygen atoms of basal carbonates by the residing  $\text{Na}^+$  cations. Further, we noticed the sulfate-mediated pairing of BA molecules to the  $\text{Na}^+$  layer, which in effect intensifies surface adsorption of BA. However, BA- $\text{SO}_4^{2-}$  interaction is considerably reduced by magnesium cations shielding sulfate sites in the  $\text{Mg}^{2+}$ -augmented brine. The findings presented in this study are of fundamental importance to advance our microscopic understanding on interfacial interactions in brine/oil/carbonate systems; with broad scientific and applied implications in the context of mobilizing organic contaminants trapped in aquifer sediments and enhancement of hydrophilicity of subsurface oil-bearing carbonate reservoirs by injecting ion-modified brine solutions.

**Keywords:** Calcite; Brine; Interface; Molecular dynamics simulation; Surface charge; Adsorption; Wettability.

# TOC Graphic



## 1. Introduction

Minerals are known to develop surface charge upon immersion in an aqueous solution<sup>1</sup>. Such charging processes lead to specific interfacial interaction affecting the structure and arrangement of the nearby surrounding fluids<sup>2</sup>. In particular, the capacity of natural minerals to adsorb organic molecules is strongly salinity-dependent, controlling processes such as bio-mineralization, contaminant migration in subsurface aquifers and wettability alteration of hydrocarbon reservoirs<sup>3</sup>. Among numerous types of mineral, calcite ( $\text{CaCO}_3$ ) is of paramount importance in diverse fields of science and technology<sup>4</sup>. Many rocks naturally occurring in the Earth's crust and ocean sediments, including limestone and chalks, are comprised of calcite<sup>5</sup>. To date, numerous investigations have shed light on the importance of surface-specific interactions of calcite-aqueous solutions, for instance, in bio-mineralization<sup>6</sup>, binding strength of organic molecules, such as methanoic acid<sup>7</sup>, poly acrylic acid<sup>8</sup>, and various alcohols<sup>9,10</sup>. Calcite-water interface has been the matter of extensive research since last decade<sup>11,12</sup>. Nevertheless, a complete understanding of the surface properties of carbonate minerals remains elusive, especially in contact with brines of varying compositions.

To date, a body of laboratory evidence has demonstrated the ion-specific interfacial characteristics of carbonates<sup>13</sup>; of practical consideration in retention of non-aqueous phase liquids (NAPLs) in aquifers, transport of organic contaminants through soil, and also increasing the oil recovery efficiency through injection of ion-modified saline solutions into petroleum reservoirs<sup>14</sup>. The latter, known as ion-tuned waterflooding (ITW), has emerged as a promising and environment-friendly technology for enhancing oil production from underground reservoirs<sup>15</sup>. Through this approach, the surface characteristics of rock-oil-brine systems, such as wettability, are optimized for oil release by adjusting (modifying) the ionic composition of the injecting brine solution<sup>16</sup>. Up to now, numerous investigations have been performed on ITW<sup>2,13,17</sup>; nevertheless, a detailed atomistic picture of that process remains unclear<sup>18</sup>. This lack of knowledge mainly stems from the inherent challenge in direct probing

nano-scale features of rock-brine interfaces<sup>18</sup>. Owing to limits of analytical methods, atomistic simulation has utilized as a powerful tool for scrutinizing contribution of ions to interface of rock/oil/brine systems with sub-nanometer resolution<sup>19–22</sup>. By applying molecular dynamics (MD) simulation, Badizad et al. figured out distinct propensity of ions for approaching and localizing in the hydrocarbon-brine interfaces<sup>23</sup>. Concerning calcite-brine systems, MD simulations carried out by Koleini et al. revealed the monotonic decrease of calcite surface charge upon diluting brine salinity<sup>24</sup>. Chen et al. demonstrated that ions could effectively screen attachment of carbohydrate monomers to the calcite surfaces,<sup>25</sup> while Liu et al. showed that organic molecules are less prone to be adsorbed on the surface of Mg-doped calcites<sup>26</sup>. By performing first-principle calculations, Liu et al.<sup>27</sup> suggested that surface population of Na<sup>+</sup> and Cl<sup>-</sup> ions nearby the calcite could potentially enhance detachment of organic molecules, hence turning wettability to weakly water-favoring condition<sup>27</sup>. In an analogous study, Sanchez and Miranda showed the ability of Mg<sup>2+</sup> to destabilize hydrocarbons pre-adsorbed onto CaCO<sub>3</sub> surfaces<sup>28</sup>, which was then verified by experimental study<sup>29</sup>.

The above-mentioned studies underline the utility of atomistic modelling for exploring surface characteristics of ion-mineral-hydrocarbons. However, given the potential complexity of such systems, fully resolving the role of individual ions at calcite-brine interfaces is still an ongoing research area. To our knowledge, no systematic investigation has ever been carried out to resolve in atomic detail the mutual interplay of ions and polar organic compounds at calcite surfaces exposed to multi-component electrolyte solutions. Here, MD simulation was undertaken to recognize how major constituting ions of natural saline waters regulate the charge density and adsorption capacity of the calcite surface. In what follows, firstly, the simulation methodology is concisely explained. Then, the surface structuring, distribution and pairwise interaction of different species are evaluated through several analyses, followed by discussing implications of this study. We hope the results obtained in this work provide

fundamental insight into the importance of water chemistry in the mechanism of charge development at calcite surfaces in geochemical environments and also ion-specific binding of polar organic constituents onto calcite surface naturally found in porous rocks constituting subsurface aquifers and oil resources.

## 2. Simulation

### 2.1 Model construction

Molecular dynamics simulation (MD) was employed to study symbiotic behavior of ions and polar hydrocarbons inside a calcite slit at various brine compositions. Two  $\text{CaCO}_3$  slabs, with dimensions of  $56.67 \text{ \AA} \times 54.89 \text{ \AA} \times 19.77 \text{ \AA}$  ( $L_x \times L_y \times L_z$ ), were placed 6 nm apart parallel to each other (orthogonal to z-direction) to form interfaces with the aqueous solution. Each slab was cleaved at the  $(10\bar{1}4)$  plane, which is the most stable and abundant polymorph of  $\text{CaCO}_3$  in the nature<sup>30–32</sup>.

In this study, Benzoic acid (BA) represents the polar fraction of natural organic matters, like crude oil, found in underground petroleum and water resources. BA has been typically utilized as in empirical and numerical investigations for modeling adsorption of polar hydrocarbons onto mineral surfaces<sup>33–35</sup>. Having both aromatic ring and carboxylic functional group, BA accounts for key characteristic of polar fraction of crude oil<sup>36–38</sup>. In each simulated model, 24 BA molecules were placed in an ordered arrangement in the middle of the slit pore (**Figure S1**, Supporting Information). Next, the interlayer spacing was filled in by 6183 water molecules, using the PACKMOL package, to achieve a water density of approximately  $1 \text{ g.cm}^{-3}$ <sup>39</sup>. Ions were introduced randomly to attain desired brine composition.

In line with typical composition of aqueous solutions used in field scale tests and lab-scale investigations<sup>29</sup>, seawater (SW, salinity of  $\sim 54.9 \text{ g.dm}^{-3}$ ) was taken as the base solution. The exact composition of SW used in this study was adopted from the frequently cited

experimental study by Yousef et al <sup>40</sup>. The role of divalent ions ( $Mg^{2+}$  and  $SO_4^{2-}$ ) was examined by modifying their concentrations with respect to a reference solution. Following the common experimental convention <sup>41–43</sup>, the concentration of divalent ions was individually increased fourfold to attain two different brines, namely, SW4Mg<sup>2+</sup> and SW4SO<sub>4</sub><sup>2-</sup>, respectively. To decouple the contribution of divalent ions, a solution solely containing Na<sup>+</sup> and Cl<sup>-</sup>, called SWNaCl, was also utilized here in the simulation. It is important to note that the total salinities of all solutions were kept constant by regulating (increasing/reducing) the NaCl concentration, as necessary. The values of ions' concentrations for each solution are listed in **Table 1**. As a complement, an ion-free solution (deionized water, DW) was considered to compare BA interaction with an ion-free CaCO<sub>3</sub> surface.

## 2.2 Interatomic potentials

The LAMMPS package was utilized to perform the MD simulations, using the velocity-Verlet scheme with a time-step of 1 fs <sup>44</sup>. The van der Waals and electrostatic interactions were calculated within the cut-off radius of 1 nm using the Lennard-Jones 12-6 (LJ) and Coulomb expressions, respectively <sup>45</sup>:

$$E_{LJ+Coul} = \left[ \frac{A_{ij}}{r_{ij}^{12}} - \frac{B_{ij}}{r_{ij}^6} \right] + \frac{e^2}{4\pi\epsilon_0} \cdot \frac{q_i q_j}{r_{ij}}, \quad (1)$$

where  $r_{ij}$  is the distance between atoms  $i$  and  $j$ .  $q$  is the partial charge valence and  $\epsilon_0$  ( $8.854 \times 10^{-12} \text{ C.V}^{-1} \text{ m}^{-1}$ ) is the vacuum permittivity. The non-bond LJ parameters ( $A_{ij}$  and  $B_{ij}$  in **Eq. 1**) between unlike atoms were described through the geometric mixing rule, that is,  $A_{ij} = \sqrt{A_{ii}A_{jj}}$  and  $B_{ij} = \sqrt{B_{ii}B_{jj}}$  <sup>46</sup>. Long-range electrostatic interactions were resolved using the particle-particle/particle-mesh (PPPM) method in the reciprocal space with the accuracy of  $10^{-5}$ . The interatomic potentials developed by Xiao et al. were adopted for modelling calcite slabs <sup>46</sup>. Consistent with the original parameterization of this force field, the water molecules were represented by the flexible TIP3P model <sup>47</sup>. Also, BA, Na<sup>+</sup>, Cl<sup>-</sup> and Mg<sup>2+</sup> were modeled using OPLS-AA force field <sup>48,49</sup>. Sulfate anions were described by the parameters developed

by Williams et al.<sup>50</sup>. Throughout, bond stretching, angle bending and dihedral rotation were described by<sup>49</sup>:

$$E_{bond} = \sum_i K_i^r (r_i - r_{i0})^2 \quad (2)$$

$$E_{angle} = \sum_i K_i^\theta (\theta_i - \theta_{i0})^2 \quad (3)$$

$$E_{dihedral} = \frac{1}{2} \sum_i \sum_{n=1}^4 K_{n,i}^\varphi [1 + (-1)^{n+1} \cos(n\varphi_i)] \quad (4)$$

where  $r_0$  and  $\theta_0$  are equilibrium bond lengths and angles, with corresponding stiffnesses of  $K^r$  and  $K^\theta$ .  $\varphi_i$  and  $K_n^\varphi$  denote dihedral angle and stiffness constants, respectively. Note that all force field parameters taken in this study are reported in Table S1 of Supporting information.

### 2.3 Simulation methodology

Each confined solution was set to 80 °C and 30 MPa, consistent with the prevailing thermodynamic conditions of many underground hydrocarbon reservoirs and aquifers<sup>51</sup>. Following the protocol described by Koleini et al.<sup>52</sup>, equilibration began by spatially constraining the bottom calcite slab and BA molecules. Brine and the top slab were coupled to the Nosé-Hoover thermostat with a damping constant of 0.1 ps. In this manner, the top calcite slab behaves as a cap floating on the beneath solution. After relaxation for 0.5 ns at 80 °C, the brine solution was compressed at the same temperature by applying a uniaxial and uniform pressure equivalent to 30 MPa at the upper calcite slab for 1.5 ns. Finally, BA molecules were allowed to move and simulation was continued for 20 ns NVT (constant number of particles, volume and temperature). Throughout, the atomic trajectories were collected every 0.5 ps and statistics extracted within the last 10.0 ns were used for post-analysis. Note that atomic configurations were captured and processed using OVITO software

<sup>53</sup>.

### 3. Results

In the following, we present various statistical analyses obtained by processing atomic trajectories. First, the equilibrium timeframe for collecting data are inferred on the basis of the mean square displacement (MSD) of BA molecules. Then, we explore the distribution and localization of water, ions and BA nearby the calcite surface; followed by radial distribution graphs to verify pairwise interactions. Finally, the spatial arrangement of ions is compared over the area of calcite-brine interfaces. Throughout, we aim to unravel the impact of brine composition on the interplay between different species in the vicinity of calcite surfaces.

#### 3.1 Mean square displacement

MSD of BA was calculated to ensure the sufficiency of the simulation timespan, given by <sup>54</sup>:

$$MSD_{\alpha}(t) = \frac{1}{N} \left\langle \sum_{i=1}^N |r_{\alpha,i}(t + t_0) - r_{\alpha,i}(t_0)|^2 \right\rangle_{t_0} \quad (5)$$

where  $r_{\alpha,i}$  is the position of a particle  $i$  along the  $\alpha$ -direction at a given instance. Summation runs over total  $N$  benzoic acids and angular brackets denote ensemble average over  $t_0$  timesteps. MSD in the parallel ( $MSD_x$  and  $MSD_y$ ) and perpendicular ( $MSD_z$ ) directions to calcite slabs were obtained for the whole timespan of the production simulations (**Figure 1**).

It can be seen in **Figure 1** that  $MSD_x$  and  $MSD_y$  increase linearly and concurrently against time, showing diffusive motion of BA molecules parallel to the solid slabs. Conversely,  $MSD_z$  diagram exhibits a sub-diffusive behavior up to  $\sim 1$  ns and levels off to a constant value at approximately 10 ns. This particular trend arises by restricted movement of BA molecules normal to the confining calcite walls. For this reason,  $MSD_z$  curves attain eventual values smaller than those of parallel counterparts,  $MSD_x$  and  $MSD_y$ . It is evident in **Figure 1** that BA molecules move around diffusively and steadily within the last 10 ns of each simulation and, hence, statistics collected during that timespan were used for further analysis.

## 3.2 Density distribution profiles

In this section we scrutinize arrangement of water, BA and ions in the calcite-brine interface on basis of density distribution profiles obtained normal to the calcite slabs (z-direction) at different compositions. Note the plane passing through the basal calcium atoms of each solid slab serves as the reference position, *i.e.* with  $z = 0$ .

### 3.2.1 Water

For any saline solution, water density profile appears oscillatory within  $\sim 1$  nm of the calcite surfaces (**Figure 2**) and beyond that, it takes a constant value, in agreement with the bulk water density,  $\sim 1 \text{ g.cm}^{-3}$ . The anomalous parts of distribution profiles identify the near-surface layering of water molecules as a result of interaction with the confining calcite slabs.<sup>55,56</sup> In these regions, localization and distribution of solutes (ions and BA) are controlled by both interplay with solid substrates and discrete water mono-layers. Snapshots captured at the end of simulation (**Figure 3**) exhibit some sort of species localization in the calcite-brine interface. Hence, in the following we analyze distribution and interaction of ions and BAs by focusing on the 1 nm-thick zone of each brine solution nearby the calcite surfaces, hereafter defined as *interface region* (**Figure 2**). As stated by Eslami and Muller-Plathe, the interface zone for a solid-liquid contact is not uniquely defined, rather it is determined on the basis of the structural or dynamical property under investigation<sup>57</sup>. This mainly originates from the conformational complicity associated with macro-molecules, like proteins or polymers, which is irrelevant to a water molecule of simple, small structure. Furthermore, we mainly dealt with species distribution perpendicular to the calcite surface, so water density profile is a natural and consistent choice for discerning interface regions.

### 3.2.2 Ions

The single, sharp peak of sodium in the number density profiles (**Figure 4**) shows that  $\text{Na}^+$  cations densely accumulate on the calcite substrate in any brine solution, between the first

and second water monolayers (indicated by vertical dashed lines in **Figure 4**). Sodium cations adhere on the calcite by inner-sphere complexation with the protruding oxygen atoms of the basal carbonates, while partly maintaining their hydration shell (note inset of **Figure 4**). By comparing height of the sodium peaks in **Figure 4** and corresponding number of comprising ions (**Table 1**), it is clear that the extent of  $\text{Na}^+$  adsorption on the calcite ( $\text{SWNaCl} > \text{SW} \approx \text{SWSO}_4^{2-} > \text{SW4Mg}^{2+}$ ) is directly proportional to its concentration in the electrolyte solution.

Chloride anions form three adsorption layers nearby the calcite surface, as distinguished in **Figure 4a**. The primary peak of  $\text{Cl}^-$  distribution (labeled 1) lies between the first and second wetting layers, overlapping the layer formed by adsorption of sodium cations on the solid substrate. Beyond that, chloride anions preferentially appear within the third water monolayer, giving rise to a further adsorption layer (labeled 2 in **Figure 4a**). In both cases, chloride anions adhere on the calcite slabs through contact ion pair (CIP)<sup>58</sup> with the pre-adhered  $\text{Na}^+$  cations. We also noticed a further peak in  $\text{Cl}^-$  distribution diagram (labeled 3), that is  $\sim 7.4$  Å above the calcite basal plane. As shown in the Inset of **Figure 4a**,  $\text{Cl}^-$  linkage to  $\text{Na}^+$  cations in this mode is mediated by peripheral water molecules, known as solvent-shared ion pairing (SSIP)<sup>58</sup>.

Overall, accumulation of chloride anions in the calcite-brine interface region is tied to  $\text{Na}^+$  cations already lodged on the calcite surface. Surface loading of chloride anions could be interpreted by thinking of the electrostatic force induced by  $\text{Na}^+$  cations covering the calcite surface. In this view,  $\text{Cl}^-$  anions are attracted towards the surface and pair with  $\text{Na}^+$  ions. Chloride anions residing beside and above the adsorbed  $\text{Na}^+$  cations lead to the first and second  $\text{Cl}^-$  layers distinguished in **Figure 4a**. We expect stronger adsorption of  $\text{Cl}^-$  ions by larger surface coverage of  $\text{Na}^+$  cations. Supporting this argument, **Figures 4a,b** and **d** show surface loading of chloride ions in brine solutions follows the order:  $\text{SWNaCl} > \text{SW} > \text{SW4Mg}^{2+}$ , despite nearly equal amount of  $\text{Cl}^-$  ions in all cases (**Table 1**).

Analogous to chlorides, sulfate anions approach the calcite surface by forming two distinct adsorption layers, as discerned in **Figure 4b**. However, peaks of sulfates are about 1 Å

beyond that of Cl<sup>-</sup>, which is possibly due to the larger size of polyatomic SO<sub>4</sub><sup>2-</sup> anion, *i.e.*, 1.8 compared to 2.4 Å<sup>59</sup>. Corresponding snapshots shown in **Figure 4b** suggest that, similar to Cl<sup>-</sup>, surface positioning of SO<sub>4</sub><sup>2-</sup> is regulated by sodium ions covering the calcite surface. It is well reflected in greater adsorption of sulfate in case of SW (**Figure 4b**) than SW4Mg<sup>2+</sup> (**Figure 4d**), because of the higher content of Na<sup>+</sup> in the former solution. Note that both solutions carry same amount of sodium cation (**Table 1**).

Amongst ions, Mg<sup>2+</sup> cations do not approach very near to the calcite surface and stay at most ~7.5 Å above the solid surface. Having a tightly bound hydration shell, penetration of magnesium cations into the compact wetting layers (**Figure 2**) incurs a large energy penalty for redistribution of its peripheral water molecules<sup>24</sup>. Moreover, the positively charged layer formed by surface coverage of Na<sup>+</sup> cations repel Mg<sup>2+</sup> ions, thus reducing their affinity for visiting the calcite-brine interface. Distribution profiles (**Figures 4c-d**) show that Mg<sup>2+</sup> ions enter the interface by especially appearing above the sulfate adsorption layers, with greatest intensity observed in the SW4Mg<sup>2+</sup> solution. Visual inspection of atom's arrangement indicates sulfate-mediated sorption of Mg<sup>2+</sup> to pre-adsorbed Na<sup>+</sup> ions (notice the inset of **Figure 4d**). Therefore, we expect the surface affinity of magnesium cations is related to number of SO<sub>4</sub><sup>2-</sup> adsorbed on the calcite substrate. The role of sulfate is well realized by not detecting magnesium in the interface of calcite-SW (**Figure 4b**). It comes with SW while having nearly same amount of Na<sup>+</sup> and Mg<sup>2+</sup> cations as SW4SO<sub>4</sub><sup>2-</sup> solution (**Table 1**).

### 3.2.3 Charge density profile

Charge density profile (**Figure 5**) quantifies the net contribution of ions, *i.e.*, combination of concentration and valence, nearby the calcite surface. It was simply obtained for each solution through valence-weighted sum of the distribution profiles of ions already presented in **Figure 4**. Despite the inherent charge neutrality of the CaCO<sub>3</sub> slabs considered in this study, the surface localization of Na<sup>+</sup> cations effectively generates a positively charged layer immediate to the calcite surface (the primary peak in **Figure 5**), with charge intensities following the

order:  $\text{SWNaCl} > \text{SW} \approx \text{SW4SO}_4^{2-} > \text{SW4Mg}^{2+}$ . The formation of such positively charged sodium layers could explain the positive zeta potential typically reported for carbonate minerals exposed to aqueous solutions <sup>60</sup>. It should be noted that calcite-brine systems modeled in this study correspond to the point of zero charge of an intact  $\text{CaCO}_3$  surface, i.e.,  $\text{pH} = 8-9$  <sup>61</sup>, which is the prevailing state of laboratory measurements and underground resources <sup>62</sup>. Therefore, at this condition, surface charge of calcite-brine arises by selective adsorption of ions.

In physical term, the adsorbed  $\text{Na}^+$  layer induces a positive electric potential and as a result, attracts anions ( $\text{Cl}^-$  and  $\text{SO}_4^{2-}$ ) toward the wetted substrate. This way, a diffuse-like negatively charged layer turns out immediate to the sodium layer (**Figure 5**). We expect the strength of the resulting negative layer is connected with the positively charged layer immediate to the calcite surface. Respecting this argument, the negative layer in  $\text{SW4Mg}^{2+}$  solution is weaker than that of SW (**Figure 5**), although both possessing nearly equal number of anions (**Table 1**). This disparity comes with the lower charge density of the positive layer in the  $\text{SW4Mg}^{2+}$  (**Figure 5**). This comparison demonstrates the extent of the negative layer is a function of the number of sodium cations covering the calcite surface. Furthermore, the lesser extent of the negative layer in the  $\text{SW4Mg}^{2+}$  solution could be partly attributed to the weaker surface activity of sulfates in the interface. This is simply inferred by absence of the doublet negative layer in the case of  $\text{SW4Mg}^{2+}$ . Varying appearance of the negative layer, for example dual peak in the case of SW and  $\text{SW4SO}_4^{2-}$  solutions, is due to different modes of surface loading of  $\text{Cl}^-$  and  $\text{SO}_4^{2-}$ . In sum, **Figure 5** verifies the formation of an electrical double layer (EDL) in the vicinity of the calcite substrate caused by biased population of anions and cations, already reported in **Figure 4**.

#### 3.2.4 Benzoic acid

Like ions, specific interactions in the interface region lead to the adherence of BA molecules on the calcite surface. Near surface anomalies of distribution profiles of BAs (**Figure 4**) reveal

the tendency of those molecules for directly binding on the solid surface. The dual peaks identified in **Figure 4c** reflect different linkage modes of BA molecules on the solid walls. In either case, an H-bond is established between carboxyl hydrogen of a BA molecule and a protruding oxygen atom of basal carbonates, which is illustrated in the pertinent snapshots (inset of **Figure 4c**). Likewise, Chen et al. pointed out H-binding adsorption of carbohydrate monomers confined within a calcite slit <sup>25</sup>. BA molecules could touch closer the calcite substrate by having their carbonyl oxygen bending towards the nearest calcium atom of the basal CaCO<sub>3</sub> plane, denoted by secondary peak in **Figure 4c**.

Varying peak heights of near-surface BA profiles (*c.f.* panels of **Figure 4**) means brine-dependent likelihood of that specie for entering the interface region and subsequently, attaching on the surface. Despite equal salinity of brine solutions (**Table 1**), it seems the surface propensity of BA molecules is connected with the ionic composition; with greatest and lowest BA adsorption occur for SW4SO<sub>4</sub><sup>2-</sup> and SW4Mg<sup>2+</sup>, respectively. From this evidence, it can be conjectured that sulfate anions enhance BA tendency for visiting the interface, whereas Mg<sup>2+</sup> acts against that affinity.

### **3.3 Radial distribution function**

Radial distribution function (RDF,  $g(r)$ ) analysis was employed to verify pairwise interactions speculated earlier on the basis of distribution profiles and selected snapshots. For calculating RDF profiles, we followed the procedure suggested by Afandak and Eslami, and Eslami et al <sup>63,64</sup>, who proposed considering those pairs falling in a cone of specified opening angle (herein 180°, or in effect a semi-spherical). Above, we argued that Na<sup>+</sup> cations tend to cover the calcite surface and meanwhile, chlorides reside in the CaCO<sub>3</sub> interface region by either adsorbing next to or above the Na<sup>+</sup> ions. RDF profiles of Na<sup>+</sup>-Cl<sup>-</sup> (**Figure 6a**) indicate that sodium and chloride ions could interact within the interface in two distinct ways. Given RDF diagram of Na<sup>+</sup>-O<sub>w</sub> (inset of **Figure 6a**), the first and second peaks labeled in **Figure 6a** are ascribed to CIP (1<sup>st</sup> and 2<sup>nd</sup> peaks **Figure 4a**) and SSIP (3<sup>rd</sup> peak in **Figure 4a**) of Na<sup>+</sup>-Cl<sup>-</sup>,

respectively. Note the MD-predicted shell radii (inset of **Figure 6a**) are consistent with hydration structure of  $\text{Na}^+$  obtained by X-ray measurements and first-principle calculations <sup>65</sup>.

It is evident in **Figure 6a** that the intensity of  $\text{Na}^+$ - $\text{Cl}^-$  pairing in the interface is evidently related to the electrolyte composition. Based on the height of RDF peaks (**Figure 6a**), the strongest sodium-chloride complexation happens in the calcite-SWNaCl interface which solely consists of  $\text{Na}^+$  and  $\text{Cl}^-$  ions. Noteworthy, the degree of  $\text{Na}^+$ - $\text{Cl}^-$  pairing reduces upon introducing other ionic species ( $\text{Mg}^{2+}$  and  $\text{SO}_4^{2-}$ ) into brine solutions, following the order: SWNaCl > SW > SW4 $\text{Mg}^{2+}$  > SW4 $\text{SO}_4^{2-}$ . The weakest  $\text{Na}^+$ - $\text{Cl}^-$  interaction observed for SW4 $\text{SO}_4^{2-}$  suggests that  $\text{SO}_4^{2-}$  anions could effectively compete with chlorides for pairing with  $\text{Na}^+$  cations in the interface, which is noticed based on  $\text{Na}^+$ - $\text{SO}_4^{2-}$  RDF (**Figure 6b**). Sulfates link to the pre-adsorbed sodiums via two intimate fashions, which is reflected in the broad (dual shoulder) peak of  $\text{Na}^+$ - $\text{SO}_4^{2-}$  RDF (**Figure 6b**). Accompanying pictures display different pairing types with sodium-sulfate in the interface, namely: bidentate (1<sup>st</sup> peak) and monodentate (2<sup>nd</sup> peak) ionic association <sup>66</sup>. As expected, the strongest sulfate-sodium binding takes place in the case of SW4 $\text{SO}_4^{2-}$  solution in which abundant sulfates have greater chance for connecting to the  $\text{Na}^+$  cations on the surface.

It was notified earlier in **Figures 4** that  $\text{Mg}^{2+}$  ions subtly load above the adsorption peak of sulfate in the distribution profiles. Visual inspection of simulation frames (**Figure 4d**) suggests that  $\text{Mg}^{2+}$  cations likely bind to sulfates in the interface. RDF profile (**Figure 6c**) demonstrates the potential interaction of  $\text{Mg}^{2+}$ - $\text{SO}_4^{2-}$  in the interface, with a sharp peak at  $\sim 4.8$  Å which is nearly at the second solvation shell of magnesium (inset of **Figure 6c**). Therefore, the  $\text{Mg}^{2+}$ - $\text{SO}_4^{2-}$  is mediated by at least a layer of peripheral water molecules, which was earlier called SSIP. This type of pairing arises by the strong hydration shell of  $\text{Mg}^{2+}$  cations which in turn inhibits their direct adsorption on  $\text{CaCO}_3$  slabs, as previously pointed out by Koleini et al. <sup>67</sup>. Overall, sulfate anions bridge  $\text{Mg}^{2+}$  cations to the  $\text{Na}^+$  ions already residing on the calcite surface.

From distribution profiles (**Figure 4**) we realized the extent of BA adsorption on the calcite substrate is a function of brine composition. Given greatest surface attachment of BA in case of SW4SO<sub>4</sub><sup>2-</sup>, one may think of the favoring interplay of BA-sulfate in the interface. This conjecture is substantiated by BA-SO<sub>4</sub><sup>2-</sup> RDF which provides a quantitative evidence on the tendency of BAs for pairing with sulfate anions already linked to Na<sup>+</sup> cations on the calcite surface (**Figure 6d**). It is evident in the clear peak of BA-SO<sub>4</sub><sup>2-</sup> RDF at ~2.8 Å. Visual inspection of timeframes further illuminates the BA-SO<sub>4</sub><sup>2-</sup> complex on the calcite surface through binding of carboxyl hydrogen of a BA to the oxygen of a sulfate ion, as elucidated in the inset of **Figure 6d**. Comparing RDF profiles at varying compositions (**Figure 6d**), it can be seen that increasing sulfate concentration promotes the BA-SO<sub>4</sub><sup>2-</sup> interaction in the interface, or in other words, BA molecules are more likely to approach the calcite surface. On the other hand, BA-SO<sub>4</sub><sup>2-</sup> binding entirely disappears in the SW4Mg<sup>2+</sup> solution, which contains highest Mg<sup>2+</sup> concentration. Recalling the Mg<sup>2+</sup>-SO<sub>4</sub><sup>2-</sup> pairing in the calcite-brine interface (**Figure 6c**), one could deduce the Mg<sup>2+</sup> cations and BA molecules compete for sulfates lodging on the calcite surface. This way, magnesium cations tend to shield uncomplexed sulfate sites at the surface and hence, inhibit attraction of BAs towards the SO<sub>4</sub><sup>2-</sup> sitting on the mineral surface. This argument is supported by having minimum amount of BA adsorption in the SW4Mg<sup>2+</sup> brine, as shown earlier in **Figure 4d**.

### **3.4 Lateral density map**

Various analyses carried out thus far signify a connection between tendency of anions (Cl<sup>-</sup> and SO<sub>4</sub><sup>2-</sup>) for localizing in the interface and the existence of a positively charged layer of Na<sup>+</sup> ions on the CaCO<sub>3</sub> surface. Lateral density map was employed as a further statistical analysis to gain an in-depth understanding of relative positioning and population of ions with respect to each other nearby the solid substrate. For this purpose, 2D distribution profiles of Na<sup>+</sup>, Cl<sup>-</sup> and SO<sub>4</sub><sup>2-</sup> ions were obtained and superimposed for different brine solution, shown in **Figure 7**.

Dense blue marks panels of **Figure 7** indicate that sodium cations firmly and individually cover the calcite surface. It is in accordance with the earlier discussion that  $\text{Na}^+$  ions prefer to reside on the protruding carbonate oxygen atoms of calcite slabs. Also, **Figure 7** clearly shows that that surface population of sodium cations correlates with the number of those ions in each brine solution (**Table 1**). As learned earlier from the ions distribution profiles (**Figure 4**),  $\text{Cl}^-$  anions partly reside immediate to the calcite surface, forming an adsorbed layer in coincidence with that of  $\text{Na}^+$  cations. This comes unexpectedly because the neutral plane of  $\text{CaCO}_3$  lacks any adsorption site for accommodating anions. Accompanying snapshots suggest the surface accumulation of chloride is assisted by pre-adsorbed  $\text{Na}^+$  cations. From a statistical viewpoint, lateral distribution maps (**Figure 7**) demonstrate  $\text{Cl}^-$  ions (yellow spots) exactly appear in portions of calcite surface populated with  $\text{Na}^+$  cations (blue spots). Together with  $\text{Na}^+-\text{Cl}^-$  RDF profile (**Figure 6a**), we conclude the primary peak of the chloride distribution profile (**Figure 4**) is due to sodium-chloride contact ion pairs formed on the calcite surface.

Analogous to  $\text{Cl}^-$  ions, spreading maps of sulfates (red points) within the interface fairly overlap with those of  $\text{Na}^+$  ions. However, unlike dense population of chlorides (yellow spots), sulfates exhibit fairly smearing distribution over the calcite surface. In conjunction with RDF (**Figure 6b**) and density distribution profiles (**Figure 4b**), this provides complementary evidence on the role of adhered sodium ions for holding sulfates in the interface region. It is worth noting that  $\text{Cl}^-$  was not detected in the lateral distribution map of  $\text{SW4SO}_4^{2-}$  (**Figure 7c**). In a same way, we shall recall that the 1<sup>st</sup> peak of  $\text{Cl}^-$  vanishes in the corresponding density distribution profile (**Figure 4c**). These together mean chloride anions in  $\text{SW4SO}_4^{2-}$  solution are not able to penetrate into the primary wetting layer of the calcite surface. It is ascribed to the negatively charged layer formed by adsorption of sulfates covering the calcite surface and consequently, repelling the chlorides from the interface region.

## 4. Discussion

So far, various analysis were employed to recognize the synergic contribution of ions to surface charging of a calcite surface and capacity of adsorbing carboxylic compounds. We focused specifically on the so-called interface region, where a few compact water layers appear in response to interaction with the calcite substrate. The MD-predicted water layering (location of maxima in the water density profile, **Figure 2**) is consistent with experimental data pointed out by Heberling et. al. <sup>32</sup>, who observed two ordered water monolayers at 2.35 and 3.34 Å above the surface calcium ions. We further noticed the appearance of charged layers by ions populating over the calcite surface. In accordance with our recent study and also learned from the MD investigation by Eslami and Muller-Plathe <sup>57</sup>, ions behavior (both spatial distribution and translation) in close to the calcite surface is expected to deviate from a homogenous bulk medium.

The open literature, particularly those concerning engineering disciplines, has been vastly devoted to experimental inspection of the contribution of divalent ions (mostly,  $Mg^{2+}$  and  $SO_4^{2-}$ ), on the wetting state of  $CaCO_3$ . In this context, special attention has been paid to divalent ions which termed potential determining ions (PDI) <sup>68</sup>. Conversely,  $Na^+$  and  $Cl^-$  ions have been widely deemed to be indifferent to the calcite surface, merely intervening in the action of PDIs <sup>69</sup>. As a major departure from this long-standing perception, the current study highlights the central role of sodium cations in regulating behavior of other ions in the calcite-brine interface. Strongly hydrated divalent ions ( $Mg^{2+}$  and  $SO_4^{2-}$ ) cannot directly bind to calcite slabs owing to a large energy penalty to be incurred upon disturbing their solvation shell and surface compact hydration layers as well <sup>70</sup>. On the contrary, a positively charged inner Helmholtz layer develops by  $Na^+$  cations penetrated into the calcite hydration layers and sitting over the oxygen atoms of the basal carbonate, as already pointed out by Ricci et al. by utilizing AFM. They observed direct attachment of  $Na^+$  ions over the topmost oxygen atoms of  $CaCO_3$  surface <sup>71</sup>. We realized surface adsorption of  $Na^+$  ions as the key for interpreting ion-specific

properties of calcite-brine interface. Despite the being inherently charged neutral, an electrical double layer is established next to the calcite surface with anions electrostatically drawn to the positively charged  $\text{Na}^+$  layer.

Surface charge density (SCD) quantifies the net contribution of ions over the calcite surface (in units of Coulomb per square meter,  $\text{C}\cdot\text{m}^{-2}$ ), which was obtained by integrating corresponding charge distribution profiles, already presented in **Figure 5**. As seen in **Figure 8**, the large and positive SCD of calcite-SWNaCl solution is in accord with the general notion that carbonate minerals typically carry positive charges upon contacting a saltwater <sup>16</sup>. **Figure 8** shows that the magnitude and even sign of the surface charge critically depends on the brine composition. This turns out while having saline solutions of same salinity (**Table 1**). Noticeably, SCD reduces upon introducing sulfates into the brine (for SW and SW4Mg<sup>2+</sup>), and even becomes negative for SW4SO<sub>4</sub><sup>2-</sup>. In an exhaustive empirical investigation by Mahrouqi et al., they pointed out that zeta potential of  $\text{CaCO}_3$  inversely correlates with the sulfate concentration of the electrolyte solution <sup>72</sup>. Considering both numerical and empirical evidence, we realize the overscreening of calcite surface by adsorption of  $\text{SO}_4^{2-}$  could turn the SCD negative, **Figure 8**. Surface charge reversal of  $\text{CaCO}_3$  surface at extra concentration of  $\text{SO}_4^{2-}$  possibly acts in favor of EDL. Throughout this mechanism, changing SCD towards negative values results in expansion and stabilization of the thin (nano-sized) brine film separating crude oil contained occupying the underground rocks from the pore walls <sup>19</sup>. Future works will assess the molecular details of EDL expansion in response to brine composition.

MD simulations showed that direct binding of BA onto calcite is connected with the number of free adsorption sites on the solid surface, that is, the protruding oxygen atoms of basal carbonates not occupied by  $\text{Na}^+$  cations. In support of this argument, we observed excessive adsorption of BA on a calcite surface exposed to DW, (**Figures S2-3**). Our deduction is qualitatively consistent with the recent study by Zhao et al., who pointed out smaller contact angle of an n-decane droplet residing on a  $\text{CaCO}_3$  substrate upon increasing salinity of the

surrounding NaCl solution <sup>73</sup>. They concluded that introducing more NaCl promotes hydrophilic virtue of a calcite surface. Also, a recent theoretical study by Li *et al.* demonstrated the key role of sodium ion in controlling wettability of calcite surfaces <sup>74</sup>. Chen *et al.* pointed out a so-called screening effect whereby salt layers formed on a calcite surface diminishes the adsorption capacity of the substrate for carbohydrate monomers <sup>25</sup>. In practical terms, using too diluted (or sodium-deficient) electrolyte solutions might give rise to severe retention of polar oil compounds into the porous carbonate minerals.

To further evaluate surface affinity of BA, the average number of the molecule visited the interface region was obtained for each brine solution and presented in **Figure 9**. This was achieved for each brine by counting and time-averaging number of benzoic acids entered into the interface regions (already defined in **Figure 2**). Note that each benzoic acid was spatially described by the positional coordinates of the carbon atom bonded to oxygen atoms of the carboxylic functional group. As seen, the tendency of BA for visiting the interface clearly depends on the ionic composition of the brine, with strongest and weakest intensities due to SW4SO<sub>4</sub><sup>2-</sup> and SW4Mg<sup>2+</sup>, respectively. BA-SO<sub>4</sub><sup>2-</sup> pairing is a major incentive for driving BA molecules to the interface. However, there would be less number of vacant sulfates on the calcite surface upon introducing extra Mg<sup>2+</sup> to the solution, by having the lowest number of BA detected in the interface of SW4Mg<sup>2+</sup> (**Figure 9**).

Altogether, sulfate takes the role of adsorption site for holding BA in the calcite-brine interface, whereas magnesium goes against this action by shielding free sulfates. It should be emphasized the present nanoscopic results are in line with empirical observations made in previous studies. For instance, Karoussi and Hamouda probed adhesion of a fatty acid on carbonate surfaces and pointed out that increasing magnesium content alters rock wettability towards more water-wet state <sup>75</sup>. This provides us with the practical implication that the brine solution injected into carboxylic dominated oil reservoirs should be enriched with magnesium cations.

## 5. Conclusions

This research is an attempt to gain atomistic insight into interplay of ions and polar hydrocarbons at the interface of  $\text{CaCO}_3$ -electrolyte solutions, with technical relevance to ion-tuned waterflooding: an operation for improving oil recovery by modulating wettability of underground reservoirs. Molecular dynamics simulation was applied to scrutinize distribution and pairwise interaction of water, ions and BA molecules nearby a calcite ( $10\bar{1}4$ ) plane in contact with various saline solutions of equal salinity.

Our study revealed the ability of sodium cations for penetrating into the compact wetting layers over the calcite surface and sit at apical oxygen atoms of basal carbonates. The resulting  $\text{Na}^+$  layer provides an explanation for positively charged surface of carbonates typically reported by experimental measurements. Also, the surface-lodging sodium cations act as anchoring sites for hosting  $\text{Cl}^-$  and  $\text{SO}_4^{2-}$  at the interface, whereas diminishing the likelihood of direct linkage of BA molecules to the basal carbonate groups. Thus, in contrast to the long-standing perception,  $\text{Na}^+$  cation is not indifferent to the calcite-brine interface, rather it critically contributes to the surface character of hydrated carbonates. In keep with empirical observations, sulfate adsorption drastically reduces surface charge and even renders calcite surface negatively charged in case of extra concentration of  $\text{SO}_4^{2-}$ , *i.e.*,  $\text{SW4SO}_4^{2-}$ . Moreover, sulfate promotes adsorption of carboxylic hydrocarbons on calcite substrates, while magnesium mitigates this effect. In practical terms, injecting an  $\text{Mg}^{2+}$ -enriched brine solution into carbonate reservoirs would potentially shift the wetting state towards water-favoring condition.

## References

- 1 K. Kobayashi, Y. Liang, S. Murata, T. Matsuoka, S. Takahashi, K. I. Amano, N. Nishi and T. Sakka, Stability Evaluation of Cation Bridging on Muscovite Surface for Improved Description of Ion-Specific Wettability Alteration, *J. Phys. Chem. C*, , DOI:10.1021/acs.jpcc.6b12116.
- 2 T. Underwood, V. Erastova, P. Cubillas and H. C. Greenwell, Molecular dynamic simulations of montmorillonite organic interactions under varying salinity: An insight into enhanced oil recovery, *J. Phys. Chem. C*, , DOI:10.1021/acs.jpcc.5b00555.
- 3 H. Du and J. D. Miller, Interfacial water structure and surface charge of selected alkali chloride salt crystals in saturated solutions: A molecular dynamics modeling study, *J. Phys. Chem. C*, , DOI:10.1021/jp071702e.
- 4 P. Fenter and N. C. Sturchio, Calcite (1 0 4)--water interface structure, revisited, *Geochim. Cosmochim. Acta*, 2012, **97**, 58–69.
- 5 B. Zhu, X. Xu and R. Tang, Hydration layer structures on calcite facets and their roles in selective adsorptions of biomolecules: A molecular dynamics study, *J. Chem. Phys.*, , DOI:10.1063/1.4848696.
- 6 C. L. Freeman, Q. Hu, M. H. Nielsen, J. Tao, J. J. De Yoreo and J. H. Harding, Surface selectivity of calcite on self-assembled monolayers, *J. Phys. Chem. C*, , DOI:10.1021/jp312108j.
- 7 C. L. Freeman, I. Asteriadis, M. Yang and J. H. Harding, *J. Phys. Chem. C*, 2009, 113, 3666–3673.
- 8 D. J. Sparks, M. E. Romero-González, E. El-Taboni, C. L. Freeman, S. A. Hall, G. Kakonyi, L. Swanson, S. A. Banwart and J. H. Harding, Adsorption of poly acrylic acid onto the surface of calcite: An experimental and simulation study, *Phys. Chem.*

- Chem. Phys.*, , DOI:10.1039/c5cp00945f.
- 9 N. Bovet, M. Yang, M. S. Javadi and S. L. S. Stipp, Interaction of alcohols with the calcite surface, *Phys. Chem. Chem. Phys.*, , DOI:10.1039/c4cp05235h.
  - 10 K. K. Sand, J. D. Rodriguez-Blanco, E. Makovicky, L. G. Benning and S. L. S. Stipp, Crystallization of CaCO<sub>3</sub> in water-Alcohol mixtures: Spherulitic growth, polymorph stabilization, and morphology change, *Cryst. Growth Des.*, , DOI:10.1021/cg2012342.
  - 11 M. Wolthers, D. Di Tommaso, Z. Du and N. H. De Leeuw, Calcite surface structure and reactivity: Molecular dynamics simulations and macroscopic surface modelling of the calcite-water interface, *Phys. Chem. Chem. Phys.*, , DOI:10.1039/c2cp42290e.
  - 12 D. Di Tommaso and N. H. De Leeuw, Structure and dynamics of the hydrated magnesium ion and of the solvated magnesium carbonates: Insights from first principles simulations, *Phys. Chem. Chem. Phys.*, , DOI:10.1039/b915329b.
  - 13 J. J. Sheng, *J. Pet. Sci. Eng.*, 2014, 120, 216–224.
  - 14 A. Rezaeidoust, T. Puntervold, S. Strand and T. Austad, Smart water as wettability modifier in carbonate and sandstone: A discussion of similarities/differences in the chemical mechanisms, *Energy and Fuels*, 2009, **23**, 4479–4485.
  - 15 J. Hao, S. Mohammadkhani, H. Shahverdi, M. N. Esfahany and A. Shapiro, *J. Pet. Sci. Eng.*, 2019.
  - 16 A. H. Saeedi Dehaghani and M. H. Badizad, Impact of ionic composition on modulating wetting preference of calcite surface: Implication for chemically tuned water flooding, *Colloids Surfaces A Physicochem. Eng. Asp.*, , DOI:10.1016/j.colsurfa.2019.02.009.
  - 17 T. Underwood, V. Erastova and H. C. Greenwell, Wetting Effects and Molecular Adsorption at Hydrated Kaolinite Clay Mineral Surfaces, *J. Phys. Chem. C*, ,

DOI:10.1021/acs.jpcc.6b00187.

- 18 P. C. Myint and A. Firoozabadi, Thin liquid films in improved oil recovery from low-salinity brine, *Curr. Opin. Colloid Interface Sci.*, 2015, **20**, 105–114.
- 19 H. Tian, F. Liu, X. Jin and M. Wang, Competitive effects of interfacial interactions on ion-tuned wettability by atomic simulations, *J. Colloid Interface Sci.*, 2019, **540**, 495–500.
- 20 M. H. Badizad, M. M. Koleini, H. C. Greenwell, S. Ayatollahi and M. H. Ghazanfari, A Deep Look into the Dynamics of Saltwater Imbibition in a Calcite Nanochannel: Temperature Impacts Capillarity Regimes, *Langmuir*, , DOI:10.1021/acs.langmuir.0c00437.
- 21 M. M. Koleini, M. H. Badizad, Z. Kargozarfard and S. Ayatollahi, Interactions between Rock/Brine and Oil/Brine Interfaces within Thin Brine Film Wetting Carbonates: A Molecular Dynamics Simulation Study, *Energy & Fuels*, 2019, **33**, 7983–7992.
- 22 M. M. Koleini, M. H. Badizad, M. H. Ghatee and S. Ayatollahi, An atomistic insight into the implications of ion-tuned water injection in wetting preferences of carbonate reservoirs, *J. Mol. Liq.*, , DOI:10.1016/j.molliq.2019.111530.
- 23 M. Hasan Badizad, M. Mehdi Koleini, R. Hartkamp, S. Ayatollahi and M. Hossein Ghazanfari, How do Ions Contribute to Brine-Hydrophobic Hydrocarbon Interfaces? An In Silico Study, *J. Colloid Interface Sci.*, , DOI:10.1016/j.jcis.2020.04.060.
- 24 M. M. Koleini, M. F. Mehraban and S. Ayatollahi, Effects of low salinity water on calcite/brine interface: A molecular dynamics simulation study, *Colloids Surfaces A Physicochem. Eng. Asp.*, 2018, **537**, 61–68.
- 25 H. Chen, A. Z. Panagiotopoulos and E. P. Giannelis, Atomistic molecular dynamics simulations of carbohydrate-calcite interactions in concentrated brine, *Langmuir*,

- 2015, **31**, 2407–2413.
- 26 H. Tomono, H. Nada, F. Zhu, T. Sakamoto, T. Nishimura and T. Kato, Effects of Magnesium Ions and water molecules on the structure of amorphous Calcium Carbonate: A molecular dynamics study, *J. Phys. Chem. B*, 2013, **117**, 14849–14856.
- 27 J. Liu, O. B. Wani, S. M. Alhassan and S. T. Pantelides, Wettability Alteration and Enhanced Oil Recovery Induced by Proximal Adsorption of Na<sup>+</sup>, Cl<sup>-</sup>, Ca<sup>2+</sup>, Mg<sup>2+</sup>, and SO<sub>4</sub><sup>2-</sup> Ions on Calcite, *Phys. Rev. Appl.*, 2018, **10**, 34064.
- 28 V. M. Sánchez and C. R. Miranda, *Modeling acid oil component interactions with carbonate reservoirs: A first-principles view on low salinity recovery mechanisms*, 2014, vol. 118.
- 29 S. Rashid, M. S. Mousapour, S. Ayatollahi, M. Vossoughi and A. H. Beigy, Wettability alteration in carbonates during “Smart Waterflood”: Underling mechanisms and the effect of individual ions, *Colloids Surfaces A Physicochem. Eng. Asp.*, , DOI:10.1016/j.colsurfa.2015.09.067.
- 30 P. Fenter and N. C. Sturchio, Calcite (104)-water interface structure, revisited, *Geochim. Cosmochim. Acta*, 2012, **97**, 58–69.
- 31 P. Fenter, S. Kerisit, P. Raiteri and J. D. Gale, Is the calcite-water interface understood? Direct comparisons of molecular dynamics simulations with specular X-ray reflectivity data, *J. Phys. Chem. C*, 2013, **117**, 5028–5042.
- 32 F. Heberling, T. P. Trainor, J. Lützenkirchen, P. Eng, M. A. Denecke and D. Bosbach, Structure and reactivity of the calcite--water interface, *J. Colloid Interface Sci.*, 2011, **354**, 843–857.
- 33 S. Mohammed and G. Gadikota, The role of calcite and silica interfaces on the aggregation and transport of asphaltenes in confinement, *J. Mol. Liq.*, 2019, **274**,

- 792–800.
- 34 F. C. D. A. Lima, R. D. S. Alvim and C. R. Miranda, From Single Asphaltenes and Resins to Nanoaggregates: A Computational Study, *Energy & Fuels*, 2017, **31**, 11743–11754.
  - 35 G. Garcia-Olvera, T. M. Reilly, T. E. Lehmann and V. Alvarado, Effects of asphaltenes and organic acids on crude oil-brine interfacial visco-elasticity and oil recovery in low-salinity waterflooding, *Fuel*, 2016, **185**, 151–163.
  - 36 S. Mohammed and G. Gadikota, The influence of CO<sub>2</sub> on the structure of confined asphaltenes in calcite nanopores, *Fuel*, 2019, **236**, 769–777.
  - 37 T. R. Zeitler, J. A. Greathouse, R. T. Cygan, J. T. Fredrich and G. R. Jerauld, Molecular Dynamics Simulation of Resin Adsorption at Kaolinite Edge Sites: Effect of Surface Deprotonation on Interfacial Structure, *J. Phys. Chem. C*, 2017, **121**, 22787–22796.
  - 38 M. Moradi, E. Topchiy, T. E. Lehmann and V. Alvarado, Impact of ionic strength on partitioning of naphthenic acids in water-crude oil systems - Determination through high-field NMR spectroscopy, *Fuel*, 2013, **112**, 236–248.
  - 39 L. Martínez, R. Andrade, E. G. Birgin and J. M. Martínez, Software News and Update Packmol: A Package for Building Initial Configurations for Molecular Dynamics Simulations, *J. Comput. Chem.*, 2009, **30**, 2157–2164.
  - 40 A. A. Yousef, S. H. Al-Saleh, A. Al-Kaabi and M. S. Al-Jawfi, Laboratory Investigation of the Impact of Injection-Water Salinity and Ionic Content on Oil Recovery From Carbonate Reservoirs, *SPE Reserv. Eval. Eng.*, 2011, **14**, 578–593.
  - 41 M. Shirazi, J. Farzaneh, S. Kord and Y. Tamsilian, Smart water spontaneous imbibition into oil-wet carbonate reservoir cores: Symbiotic and individual behavior of

- potential determining ions, *J. Mol. Liq.*, , DOI:10.1016/j.molliq.2019.112102.
- 42 S. Moradi, A. A. Isari, Z. Bachari and H. Mahmoodi, Combination of a new natural surfactant and smart water injection for enhanced oil recovery in carbonate rock: Synergic impacts of active ions and natural surfactant concentration, *J. Pet. Sci. Eng.*, , DOI:10.1016/j.petrol.2019.01.043.
- 43 A. H. S. Dehaghani, M. Hosseini, A. Tajikmansori and H. Moradi, A mechanistic investigation of the effect of ion-tuned water injection in the presence of cationic surfactant in carbonate rocks: An experimental study, *J. Mol. Liq.*, , DOI:10.1016/j.molliq.2020.112781.
- 44 Steve Plimton, Fast Parallel Algorithms for Short-Range Molecular Dynamics, *J. Comput. Phys.*, 1995, **117**, 1–19.
- 45 D. Frenkel and B. Smit, *Understanding molecular simulation: From algorithms to applications*, 1996.
- 46 S. Xiao, S. A. Edwards and F. Gräter, A new transferable force-field for simulating the mechanics of CaCO<sub>3</sub> crystals, *J. Phys. Chem. C*, 2011, **115**, 20067–20075.
- 47 W. L. Jorgensen, J. Chandrasekhar, J. D. Madura, R. W. Impey and M. L. Klein, Comparison of simple potential functions for simulating liquid water, *J. Chem. Phys.*, 1983, **79**, 926–935.
- 48 W. Damm, A. Frontera, J. Tirado-Rives and W. L. Jorgensen, OPLS all-atom force field for carbohydrates, *J. Comput. Chem.*, 1997, **18**, 1955–1970.
- 49 W. L. Jorgensen, D. S. Maxwell and J. Tirado-Rives, Development and testing of the OPLS all-atom force field on conformational energetics and properties of organic liquids, *J. Am. Chem. Soc.*, , DOI:10.1021/ja9621760.
- 50 C. D. Williams, N. A. Burton, K. P. Travis and J. H. Harding, The Development of a

- Classical Force Field To Determine the Selectivity of an Aqueous Fe<sup>3+</sup>–EDA Complex for TcO<sub>4</sub><sup>-</sup> and SO<sub>4</sub><sup>2-</sup>, *J. Chem. Theory Comput.*, 2014, **10**, 3345–3353.
- 51 T. H. Ahmed, *Reservoir Engineering Handbook (Fourth Edition)*, 2010.
- 52 M. M. Koleini, M. H. Badizad, R. Hartkamp, S. Ayatollahi and M. H. Ghazanfari, The Impact of Salinity on the Interfacial Structuring of an Aromatic Acid at the Calcite/Brine Interface: An Atomistic View on Low Salinity Effect, *J. Phys. Chem. B*, 2020, **124**, 224–233.
- 53 A. Stukowski, Visualization and analysis of atomistic simulation data with OVITO-the Open Visualization Tool, *Model. Simul. Mater. Sci. Eng.*, , DOI:10.1088/0965-0393/18/1/015012.
- 54 M. H. Ghatee and M. M. Koleini, Bonding, structural and thermodynamic analysis of dissociative adsorption of H<sub>3</sub>O<sup>+</sup> ion onto calcite (10<sup>-4</sup>) surface: CPMD and DFT calculations, *J. Mol. Model.*, 2017, **23**, 331.
- 55 A. Kirch, S. M. Mutisya, V. M. Sánchez, J. M. De Almeida and C. R. Miranda, Fresh Molecular Look at Calcite-Brine Nanoconfined Interfaces, *J. Phys. Chem. C*, , DOI:10.1021/acs.jpcc.7b12582.
- 56 M. M. Koleini, M. H. Badizad and S. Ayatollahi, An atomistic insight into interfacial properties of brine nanofilm confined between calcite substrate and hydrocarbon layer, *Appl. Surf. Sci.*, 2019, **490**, 89–101.
- 57 H. Eslami and F. Müller-Plathe, How thick is the interphase in an ultrathin polymer film? Coarse-grained molecular dynamics simulations of polyamide-6,6 on graphene, *J. Phys. Chem. C*, , DOI:10.1021/jp400142h.
- 58 J. N. Israelachvili, *Intermolecular and Surface Forces: Third Edition*, 2011.
- 59 Y. Marcus, Ionic Radii in Aqueous Solutions, *Chem. Rev.*, 1988, **88**, 1475–1498.

- 60 M. D. Jackson, D. Al-Mahrouqi and J. Vinogradov, Zeta potential in oil-water-carbonate systems and its impact on oil recovery during controlled salinity water-flooding, *Sci. Rep.*, 2016, **6**, 37363.
- 61 P. Somasundaran and G. E. Agar, The zero point of charge of calcite, *J. Colloid Interface Sci.*, , DOI:10.1016/0021-9797(67)90241-X.
- 62 N. R. Pedersen, T. Hassenkam, M. Ceccato, K. N. Dalby, K. Mogensen and S. L. S. Stipp, Low Salinity Effect at Pore Scale: Probing Wettability Changes in Middle East Limestone, *Energy and Fuels*, , DOI:10.1021/acs.energyfuels.5b02562.
- 63 A. Afandak and H. Eslami, Ion-pairing and electrical conductivity in the ionic liquid 1-n-butyl-3-methylimidazolium methylsulfate [Bmim][MeSO<sub>4</sub>]: Molecular dynamics simulation study, *J. Phys. Chem. B*, , DOI:10.1021/acs.jpcc.7b06039.
- 64 H. Eslami, M. Khani and F. Müller-Plathe, Gaussian Charge Distributions for Incorporation of Electrostatic Interactions in Dissipative Particle Dynamics: Application to Self-Assembly of Surfactants, *J. Chem. Theory Comput.*, , DOI:10.1021/acs.jctc.9b00174.
- 65 M. Galib, M. D. Baer, L. B. Skinner, C. J. Mundy, T. Huthwelker, G. K. Schenter, C. J. Benmore, N. Govind and J. L. Fulton, Revisiting the hydration structure of aqueous Na<sup>+</sup>, *J. Chem. Phys.*, , DOI:10.1063/1.4975608.
- 66 L. Pegado, O. Marsalek, P. Jungwirth and E. Wernersson, Solvation and ion-pairing properties of the aqueous sulfate anion: Explicit versus effective electronic polarization, *Phys. Chem. Chem. Phys.*, , DOI:10.1039/c2cp40711f.
- 67 M. M. Koleini, M. H. Badizad, Z. Kargozarfard and S. Ayatollahi, The impact of salinity on ionic characteristics of thin brine film wetting carbonate minerals: An atomistic insight, *Colloids Surfaces A Physicochem. Eng. Asp.*, 2019, **571**, 27–35.

- 68 S. J. Fathi, T. Austad and S. Strand, Water-based enhanced oil recovery (EOR) by “smart water”: Optimal ionic composition for EOR in carbonates, *Energy and Fuels*, 2011, **25**, 5173–5179.
- 69 A. Alroudhan, J. Vinogradov and M. D. Jackson, Zeta potential of intact natural limestone: Impact of potential-determining ions Ca, Mg and SO<sub>4</sub>, *Colloids Surfaces A Physicochem. Eng. Asp.*, 2016, **493**, 83–98.
- 70 P. Schienbein, G. Schwaab, H. Forbert, M. Havenith and D. Marx, Correlations in the Solute-Solvent Dynamics Reach beyond the First Hydration Shell of Ions, *J. Phys. Chem. Lett.*, , DOI:10.1021/acs.jpcclett.7b00713.
- 71 M. Ricci, P. Spijker, F. Stellacci, J.-F. Molinari and K. Voitchovsky, Direct Visualization of Single Ions in the Stern Layer of Calcite, *Langmuir*, 2013, **29**, 2207–2216.
- 72 D. Al Mahrouqi, J. Vinogradov and M. D. Jackson, *Adv. Colloid Interface Sci.*, 2017, 240, 60–76.
- 73 J. Zhao, G. Yao and D. Wen, Salinity-dependent alterations of static and dynamic contact angles in oil/brine/calcite systems: A molecular dynamics simulation study, *Fuel*, , DOI:10.1016/j.fuel.2020.117615.
- 74 H. Li, H. Vovusha, S. Sharma, N. Singh and U. Schwingenschlögl, Mechanism of wettability alteration of the calcite {101} surface, *Phys. Chem. Chem. Phys.*
- 75 O. Karoussi and A. A. Hamouda, Macroscopic and nanoscale study of wettability alteration of oil-wet calcite surface in presence of magnesium and sulfate ions, *J. Colloid Interface Sci.*, , DOI:10.1016/j.jcis.2007.09.045.



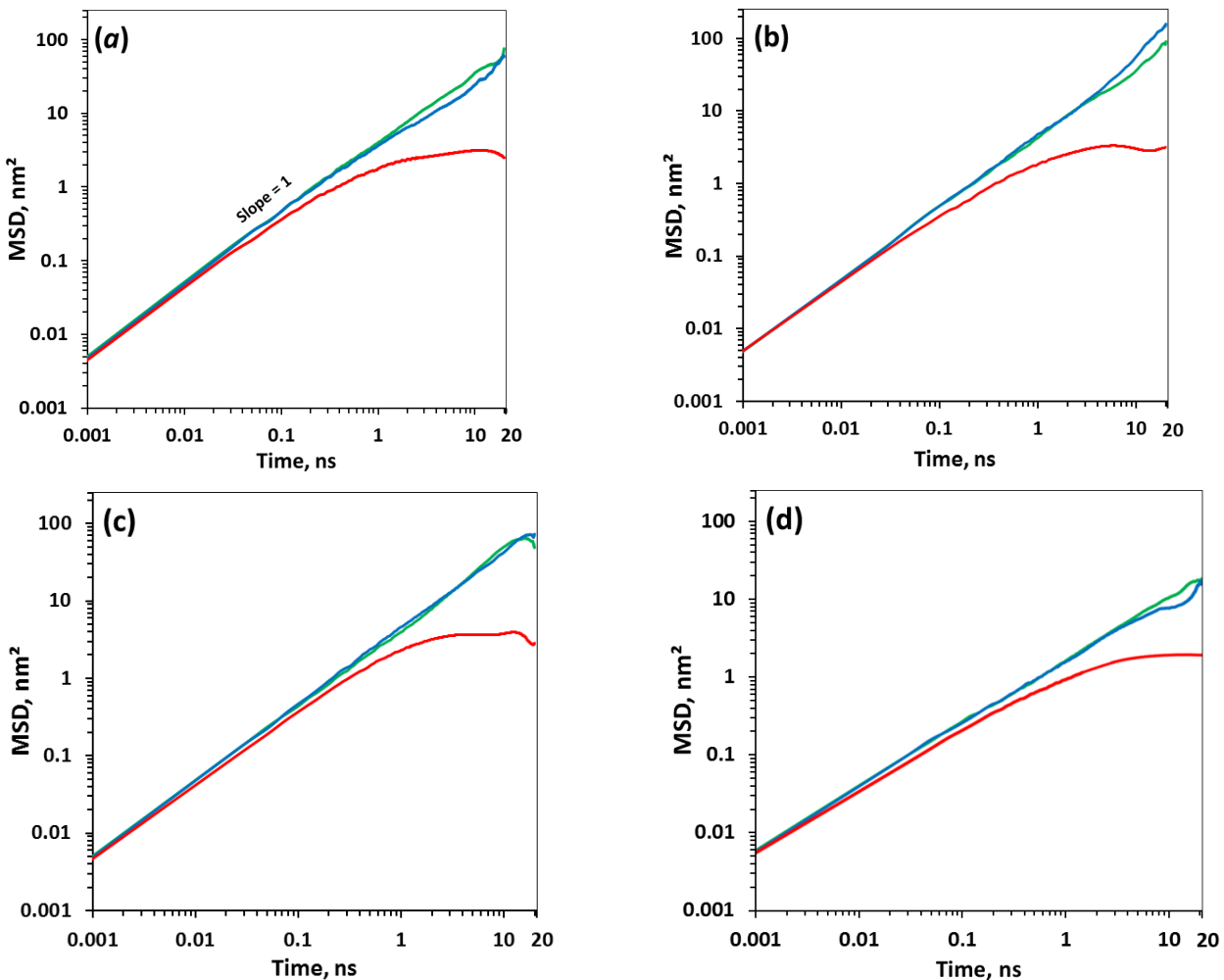


**Figure 1** Different components of mean square displacement ( $\text{MSD}_x$ : green,  $\text{MSD}_y$ : blue, and  $\text{MSD}_z$ : red) of BA molecules confined within the calcite slit at different brine solutions: (a) SWNaCl, (b) SW, (c) SW4 $\text{Mg}^{2+}$ , and (d) SW4 $\text{SO}_4^{2-}$ . All plots are in the log-log scale.

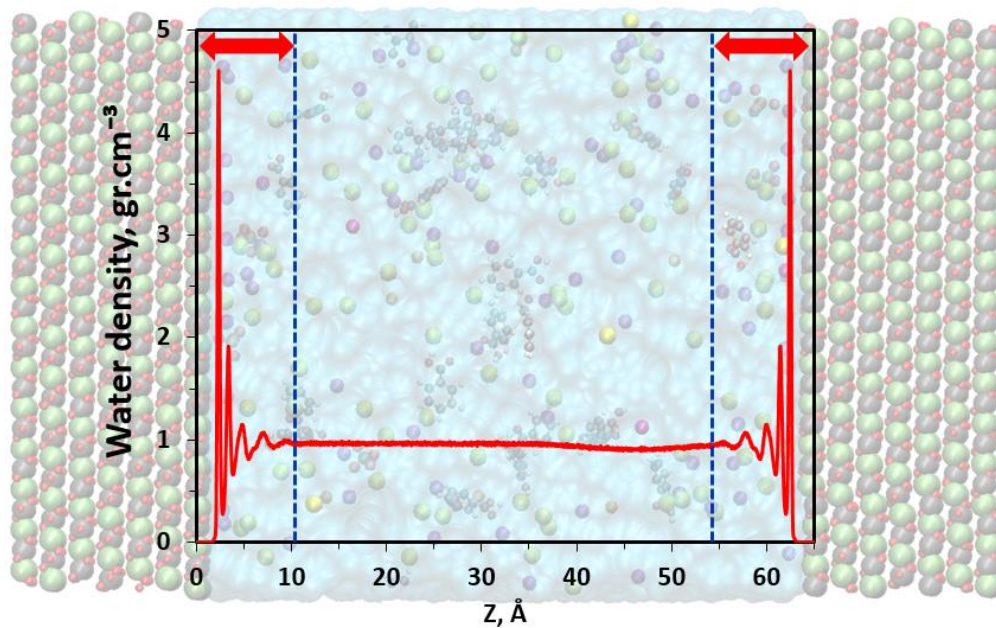


**Figure 2** Distribution of water density normal to the calcite slabs (z-direction). An exemplified snapshot of the system is shown in the background. Interface regions are identified by double arrows.

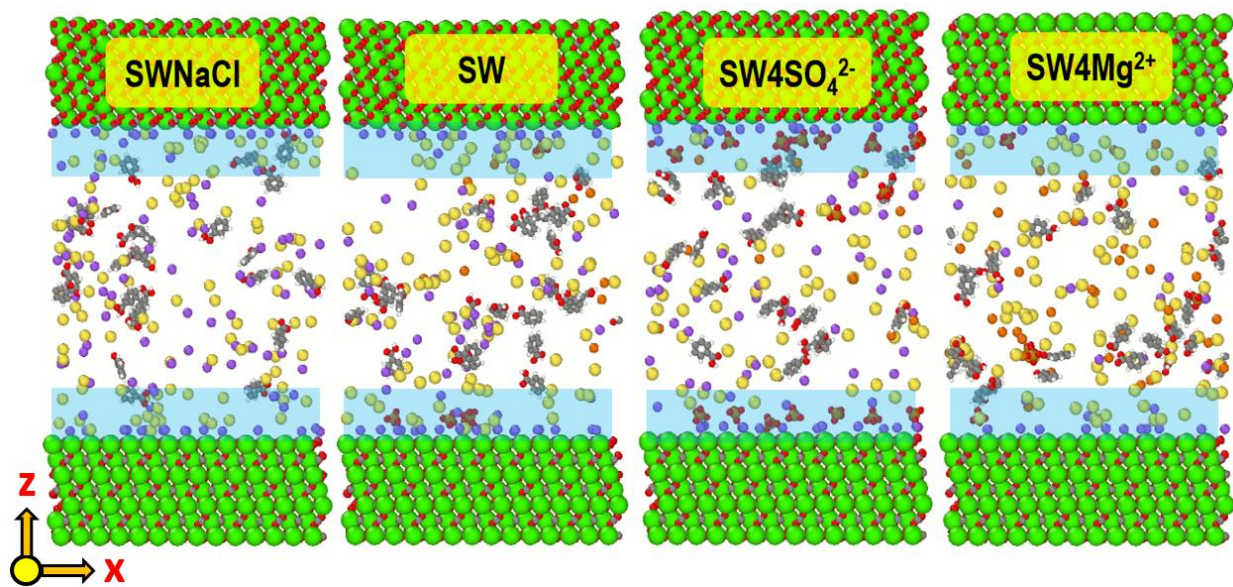


**Figure 3** Final snapshots taken for different brine solution confined within the calcite slit. Regions highlighted in blue indicate the interface, defined in the text body. The color scheme of snapshots are specified as follows. Calcite slabs are comprised of carbon (gray), oxygen (red), and calcium (green) atoms. Ions are depicted as finite size spheres, namely, sodium (purple), chloride (yellow), magnesium (orange), oxygen (red), and sulfur (dark cream). Water molecules are hidden for clarity.

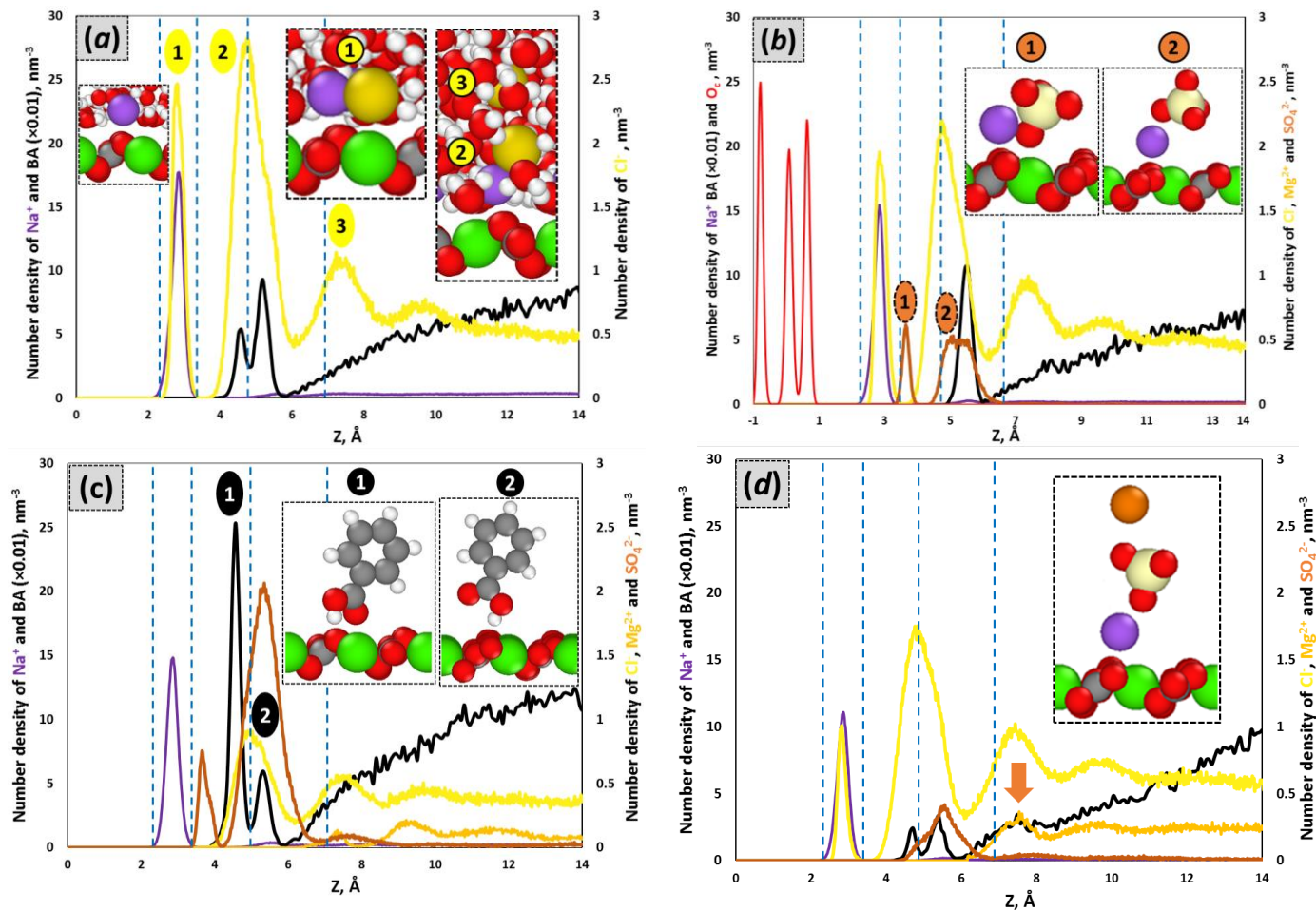


**Figure 4** Distribution profiles of  $\text{Na}^+$  (purple),  $\text{Cl}^-$  (yellow),  $\text{SO}_4^{2-}$  (brown),  $\text{Mg}^{2+}$  (orange) and BA (black) nearby the calcite surface at various electrolyte solutions: (a) SWNaCl; (b) SW; (c) SW4 $\text{SO}_4^{2-}$ ; and (d) SW4 $\text{Mg}^{2+}$ . Insets illustrate atomic configurations for corresponding adsorption layers discerned in each panel. Color codes are explained in the caption of Figure 3. The spatial distribution of the oxygen atoms of basal carbonates ( $\text{O}_c$ ) is displayed in panel (b).

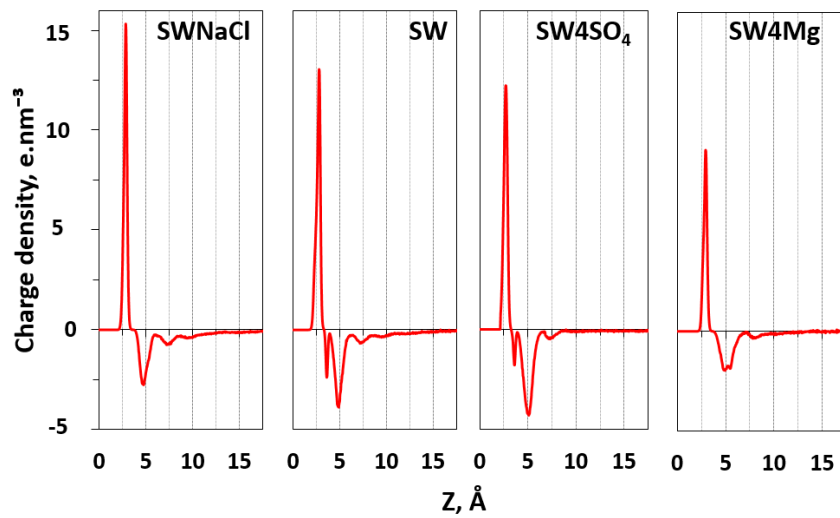


**Figure 5** Charge density distribution perpendicular to calcite surfaces (i.e., along z-axis) at various brine solutions.

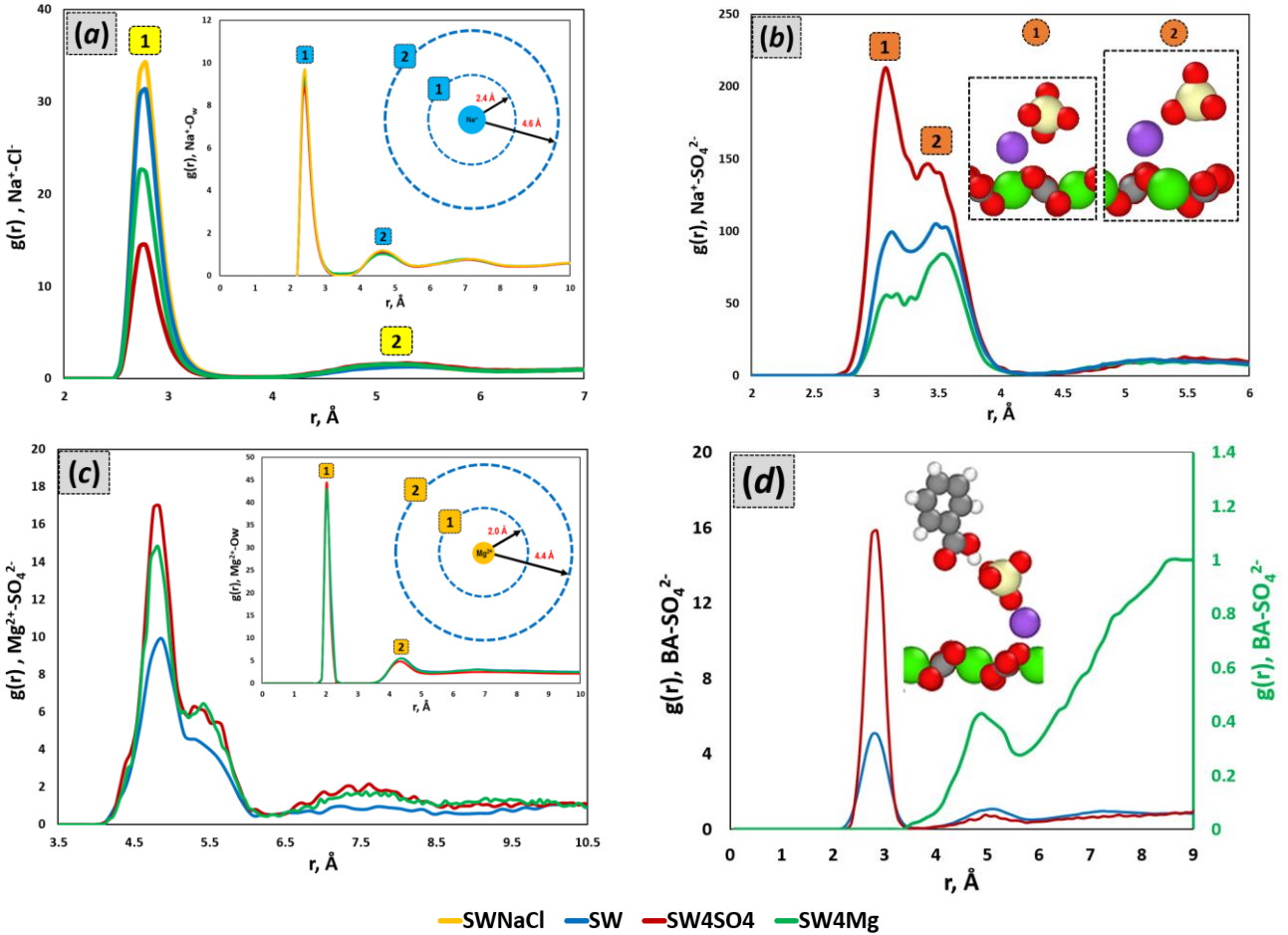


**Figure 6** RDF profile of **(a)**  $\text{Na}^+\text{-Cl}^-$ , **(b)**  $\text{Na}^+\text{-SO}_4^{2-}$ , **(c)**  $\text{Mg}^{2+}\text{-SO}_4^{2-}$ , and **(d)**  $\text{BA-SO}_4^{2-}$  in the interface of calcite-brine solutions. Insets of panels (a) and (b) show RDF profiles of solvation shell surrounding  $\text{Na}^+$  and  $\text{Mg}^{2+}$ , respectively. Insets of panels (b) and (d) illustrate different interactions modes corresponding to each. RDF profiles. Color codes are defined in the caption of Figure 3.

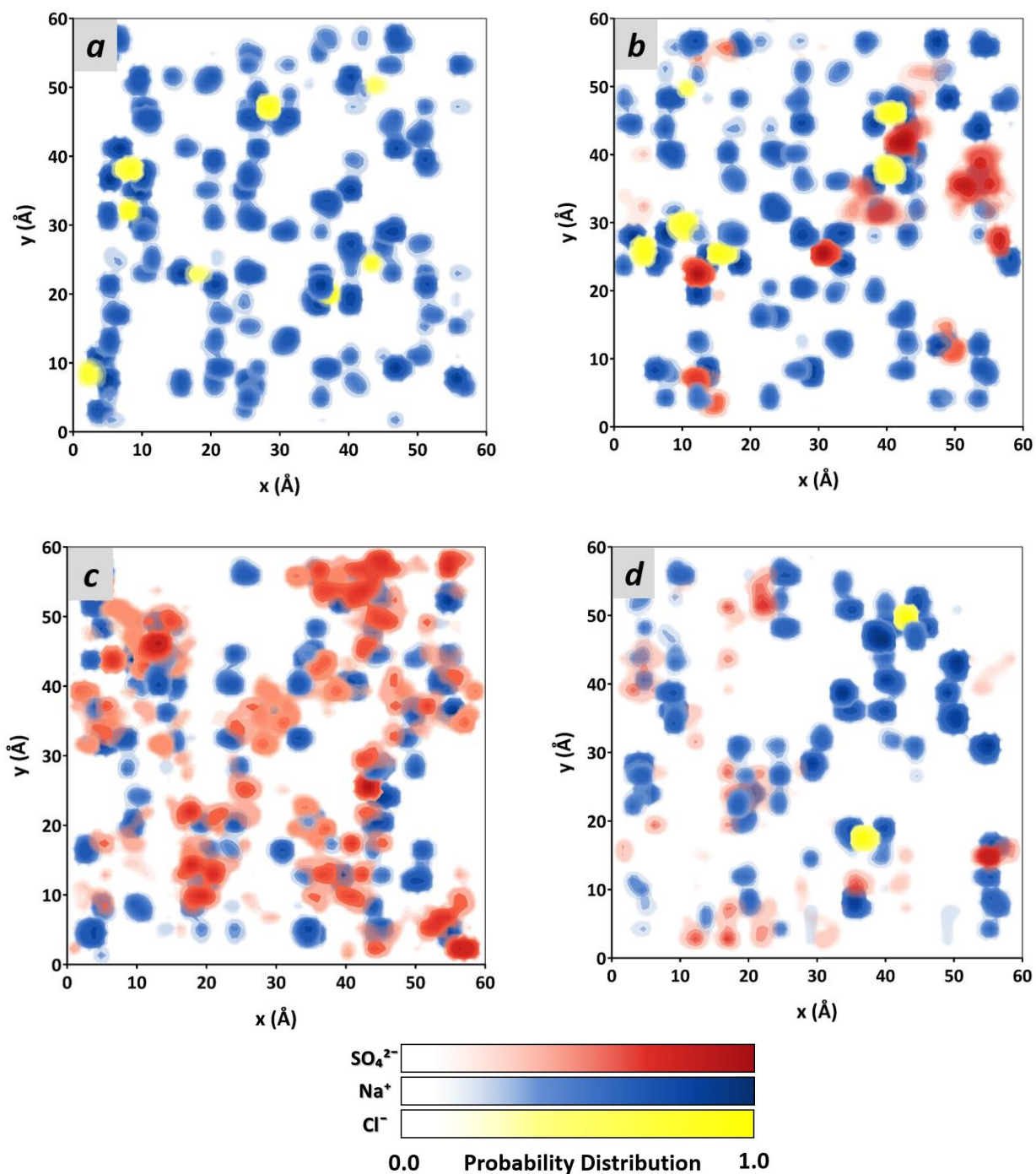


**Figure 7** Lateral distribution maps of  $\text{SO}_4^{2-}$ ,  $\text{Na}^+$  and  $\text{Cl}^-$  in the calcite-brine interface at different electrolyte contents: (a) SWNaCl; (b) SW; (c) SW4 $\text{SO}_4^{2-}$ ; and (d) SW4 $\text{Mg}^{2+}$ .

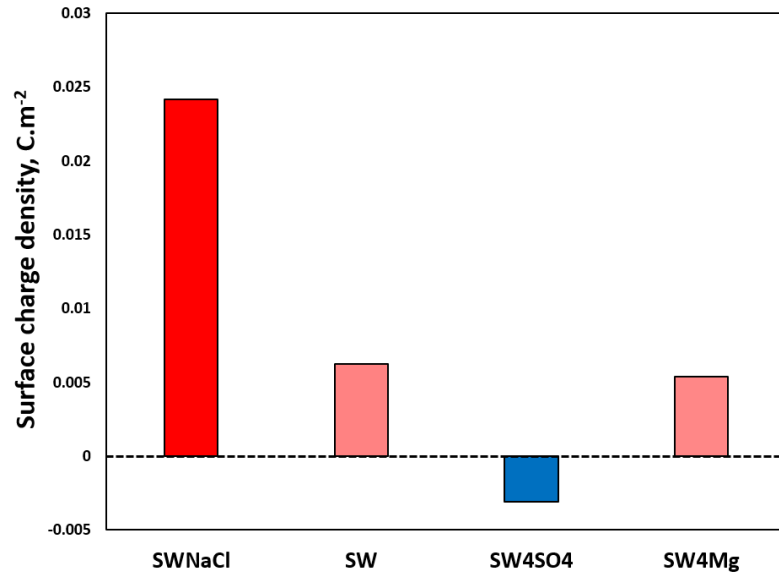


**Figure 8** Surface charge density of calcite-brine interface at various electrolyte composition.

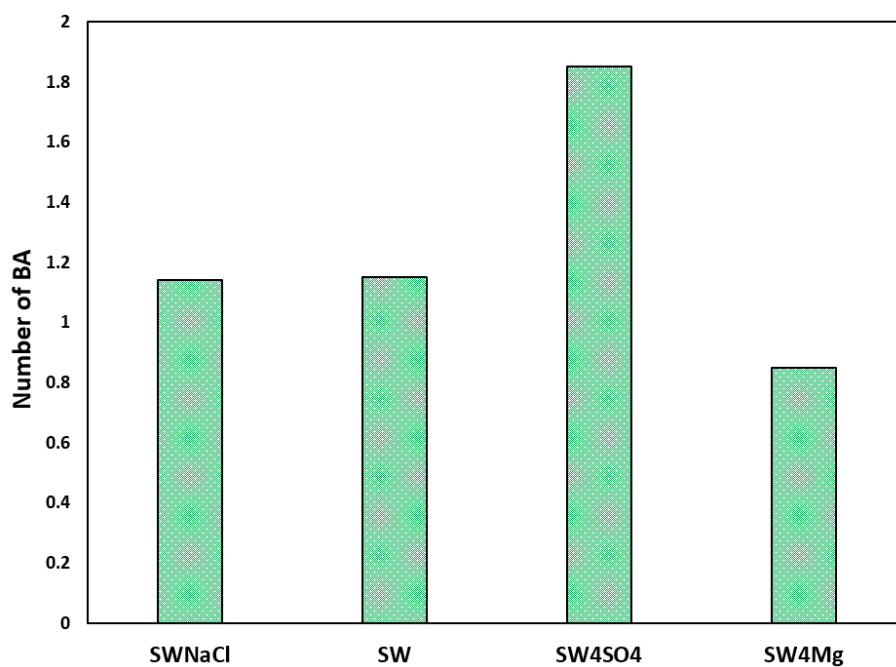


**Figure 9** Average number of BA molecules entered into interface regions at different brine compositions.

**Table 1** Number of ions comprising brine solutions in present study. Note all brines are of equal salinity,  $\sim 54.9 \text{ g.dm}^{-3}$ .

Ion	Solution			
	SWNaCl	SW	SW4SO <sub>4</sub> <sup>2-</sup>	SW4Mg <sup>2+</sup>
Na <sup>+</sup>	108	90	83	40
Cl <sup>-</sup>	108	100	63	110
Mg <sup>2+</sup>	-	10	10	40
SO <sub>4</sub> <sup>2-</sup>	-	5	20	5